

Different noncollinear magnetizations on two edges of zigzag graphene nanoribbons

Yang Xiao(肖杨)[1,†], Qiaoli Ye(叶巧利)[1,†], Jintao Liang(梁锦涛)[1], Xiaohong Yan(颜晓红)[2], and Ying Zhang(张影)[1,‡]

Citation: Chin. Phys. B, 2020, 29 (**12**): 127201. DOI: 10.1088/1674-1056/abc0e4
Journal homepage: http://cpb.iphy.ac.cn; http://iopscience.iop.org/cpb

What follows is a list of articles you may be interested in

Valley-polarized pumping current in zigzag graphene nanoribbons with different spatial symmetries

Zhizhou Yu(俞之舟), Fuming Xu(许富明)
Chin. Phys. B, 2018, 27 (**12**): 127203. DOI: 10.1088/1674-1056/27/12/127203

Transport properties of zigzag graphene nanoribbons adsorbed with single iron atom

Yang Yu-E, Xiao Yang, Yan Xiao-Hong, Dai Chang-Jie
Chin. Phys. B, 2015, 24 (**11**): 117204. DOI: 10.1088/1674-1056/24/11/117204

Adiabatic quantum pump in a zigzag graphene nanoribbon junction

Zhang Lin
Chin. Phys. B, 2015, 24 (**11**): 117202. DOI: 10.1088/1674-1056/24/11/117202

Valley selection rule in a Y-shaped zigzag graphene nanoribbon junction

Zhang Lin, Wang Jun
Chin. Phys. B, 2014, 23 (**8**): 087202. DOI: 10.1088/1674-1056/23/8/087202

Resonant tunneling through double-barrier structures on graphene

Deng Wei-Yin, Zhu Rui, Xiao Yun-Chang, Deng Wen-Ji
Chin. Phys. B, 2014, 23 (**1**): 017202. DOI: 10.1088/1674-1056/23/1/017202

Different noncollinear magnetizations on two edges of zigzag graphene nanoribbons*

Yang Xiao(肖杨)[1,†], Qiaoli Ye(叶巧利)[1,†], Jintao Liang(梁锦涛)[1], Xiaohong Yan(颜晓红)[2], and Ying Zhang(张影)[1,‡]

[1] College of Science, Nanjing University of Aeronautics and Astronautics, Nanjing 210016, China
[2] School of Material Science and Engineering, Jiangsu University, Zhenjiang 212013, China

(Received 13 July 2020; revised manuscript received 22 September 2020; accepted manuscript online 14 October 2020)

Based on density functional theory and non-equilibrium Green's function method, we studied noncollinear magnetism and spin transport in a 180° domain wall made of zigzag graphene nanoribbon (ZGNR) with different noncollinear magnetic profiles on the top and bottom edges. Our results show that a helical domain wall on the top (bottom) edge and an abrupt domain wall on the bottom (top) edge can survive in the ZGNR. This indicates that such characteristic magnetization distribution can be obtained by some means, e.g., the introduction of impurity on one edge. Compared to a wide ZGNR, a narrow ZGNR presents obvious coupling between the two edges which changes the magnetization and transmission greatly. As for the above-mentioned distinct magnetic profile, the spin transport is blocked in the abrupt domain wall due to strong spin flip scattering while remains unaffected in the helical domain wall due to the spin mixing effect. We deduce a formula of the transmission for various magnetic profiles of the ZGNRs. A new result based on this formula is that the transmission at the Fermi level can be zero, one, and two by tuning the edge magnetization. Our results provide insights into the noncollinear spin transport of the ZGNR-based devices.

Keywords: graphene nanoribbon, spintronic transport, density functional theory, nonequilibrium Green's function

PACS: 72.10.−d, 85.65.+h, 73.63.−b **DOI:** 10.1088/1674-1056/abc0e4

1. Introduction

Graphene nanoribbon has attracted much attention due to its fantastic electronic, optical, and mechanical properties which may render potential application in carbon-based nanodevices.[1–12] By cutting graphene along different direction, one can obtain nanoribbon of the armchair or zigzag type. Of them, zigzag graphene nanoribbon (ZGNR) has been extensively studied in that it shows spin-polarized electronic states.[13–23] Therefore, the ZGNR is a potential candidate for spintronic applications. In experiment, the long-distance propagation of spin has been observed.[24] In theory, the ZGNR shows a variety of spin-dependent electronic properties. For instance, the electronic states could be either symmetric or asymmetric depending on the width of the ribbon.[25] The transmission is determined by the symmetry and could be blocked by such symmetry and magnetization alignment of the left and right leads.[26]

In many experimental and theoretical studies, the magnetism of the ZGNR is usually assumed to be collinear, i.e., the magnetic moments of all atoms are aligned along the same line.[24–26] In general, noncollinear magnetism is energetically unfavorable due to the absence of competition of magnetic exchange interaction[27–29] and spin–orbit interaction.[30] However, in some special situations, noncollinear magnetism can occur. Czerner *et al.* have studied the nanojunction made of transition metal nanowire.[31] The helical domain wall is obtained by restricting two leads magnetization along the opposite directions. Here, noncollinear magnetism is energetically more favorable than the collinear one since it has the smaller magnetic exchange interaction in the domain wall. Based on this principle, zhang *et al.*[32] studied the two-probe model of the ZGNR by setting two lead magnetizations in different directions described by the twist angle θ. The twist angle is defined as the relative angle between magnetizations of the left and right leads. For a long nanoribbon, noncollinear domain wall is obtained for small twist angle but collinear domain wall is favorable for large twist angle. Moreover, at the Fermi level, the transmission coefficient remains almost constant with the twist angle varied. This interesting feature implies that small perturbation in magnetization orientation does not change the transmission greatly.

We notice that, in previous calculations, noncollinear magnetization distributions are assumed to be the same on the top and bottom edges of the ZGNR.[32] That is to say, the domain wall on the top edge is the same as that on the bottom edge. In this case, the top and bottom edges give equal contributions to electronic transmission. Based on this, it is natural to ask: What are the magnetization profile and transport properties when the top and bottom edge magnetizations are different? To answer this question, we extend the calculation in Ref. [32] to the case where magnetizations on two edges of

*Project supported by the National Natural Science Foundation of China (Grant Nos. NSFC11804158, NSFC61974067, NSFC91750112, and NSFC11947101).
†These authors contributed equally.
‡Corresponding author. E-mail: yingzhang@nuaa.edu.cn
© 2020 Chinese Physical Society and IOP Publishing Ltd

the ZGNR are not the same. Several new results and physics are discussed and revealed.

The remainder of the paper is organized as follows. In Section 2, we show the computational method and structural model of the ZGNR with different magnetizations on two edges. The construction of collinear and helical magnetizations is discussed. In Section 3, the results of magnetization distribution and transmission coefficient are given. The physical mechanisms are discussed. The findings are summarized in Section 4.

2. Computational methods and models

The calculation is performed in three steps using the OpenMX package.[33] In the first step, the structural optimization is done in order to find the energetically stable position of each atom. In the second step, a two-probe geometry containing left lead, right lead, and the central region is considered. The magnetizations of the left and right leads are fixed and the electronic states in the central region are self-consistently iterated. In the construction of the Hamiltonian, the pseudoatomic orbitals (PAOs) and norm-conserving pseudopotentials are employed in the local density approximation (LDA) of density functional theory (DFT). The PAOs for carbon and hydrogen atoms are C5.0-s2p1 and H5.0-s2p1 where 5.0 and s2p1 represent the cutoff radius (in Bohr unit) of atomic orbital and the primitive atomic orbitals used. The energy cutoff for real space integration and the solution of Poisson equation is 300 Ry. Due to the use of open boundary condition, the key physical quantity is the density matrix. We use the Hamiltonian matrix, overlap matrix, and self-energy of leads to calculate the Green's function of the central region and the density matrix based on the non-equilibrium Green's function method.[34–38] With the density matrix and atomic orbitals, the charge density is obtained and iterated until the convergence is reached. In our calculations, we set the electronic temperature at 300 K. In the third step, we use the converged quantities, i.e., the Green's function and self-energy, to calculate the transmission coefficient based on the Landauer formula.

The ZGNR under study is mirror symmetric with respect to the midplane between the two edges as shown in Fig. 1 with different widths, i.e., $N = 10$, 8, and 4. Here, N defines the number of carbon atoms in the vertical direction. The length is defined in the transport direction, i.e., $L_y = (N_{\text{edge}} - 1)a$ with $a = \sqrt{3}a_{\text{C-C}}$, where $a_{\text{C-C}}$ is the distance between two neighbouring carbon atoms. N_{edge} is the number of carbon atoms in the edges. In this work, we consider $N_{\text{edge}} = 17$. All carbon atoms on the edge are saturated with hydrogen atoms. Some buffer layers are added to the left and the right sides of the central region in order to achieve convergence.

The noncollinear magnetism is realized by setting the magnetizations of the left and right leads antiparallel, i.e., $\theta = 180^\circ$. Two spin quantization axes,[39,40] i.e., global and local axes, are used. The global axis is always along the z axis. The local axis is along the direction of each atom's magnetization, which varies from atom to atom. When the left and right lead magnetizations are fixed, the magnetization profile in the central region can be helical or collinear, i.e., a helical or abrupt domain wall. The abrupt domain wall can be almost regarded as a collinear magnetization distribution. But in the helical domain wall,[41] the local magnetic moment of carbon atom on the edge along the ZGNR rotates between two lead magnetizations in constant step of $180^\circ/(N_{\text{edge}} - 1)$. In the process of self-consistent iteration, the amplitude and direction of the magnetic moments of all atoms in the central region are fully relaxed.

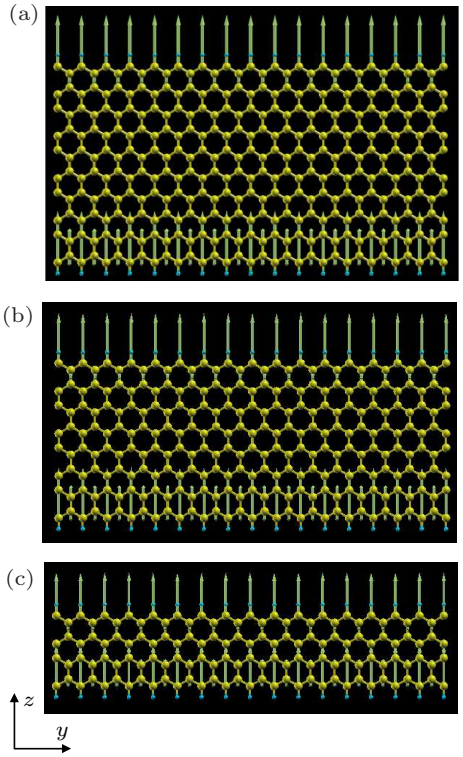


Fig. 1. Magnetization distributions of (a) $N = 10$, (b) $N = 8$, and (c) $N = 4$ ZGNRs at $\theta = 0^\circ$. θ is the angle between magnetizations of the left and right leads.

3. Results and discussion

For the sake of comparison, we first present the magnetization distribution of $\theta = 0^\circ$ shown in Fig. 1. One can clearly see a ferromagnetic order on both top and bottom edges of the nanoribbon. As the two lead magnetizations are parallel, any deviation from lead magnetization in the central region will increase the Heisenberg exchange energy. Moreover, we can notice two phenomena: (i) the magnetization of the central region is mainly arisen from the two leads; (ii) the magnetization is mainly on the edge atoms, instead of the interior atoms. The first can be attributed to the fact that a fixed boundary condition is used in our transport calculations. As the two lead

magnetizations are fixed, the magnetization in the central region can only be relaxed under such boundary condition. As the two lead magnetizations are parallel, the magnetization of the central region is forced to align in a ferromagnetic way. As for the latter behavior, the magnetization of the ZGNR is arisen from the zigzag edge for which only one of A and B sublattices appears on each edge.[14] Since the numbers of A and B sublattice atoms are equal for the interior atoms, no magnetism occurs. In Fig. 1, one can see that the magnetization distribution remains almost unchanged when shrinking the width of the ZGNR. But, this is not true for the electronic band structure and transmission coefficient.

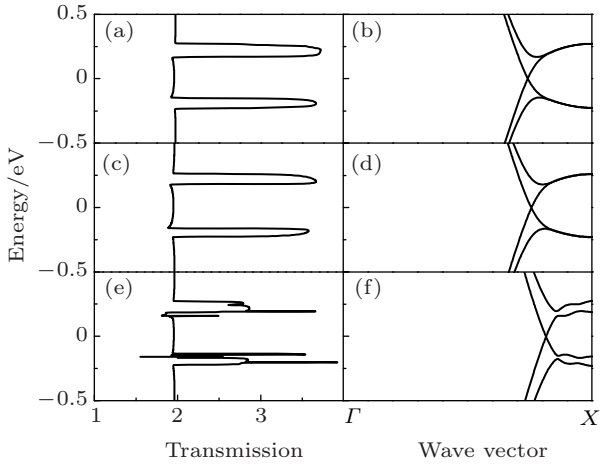


Fig. 2. (a) Transmission curve and (b) band structure of $N = 10$ ZGNR at $\theta = 0°$. (c) and (d) Those for $N = 8$ ZGNR, (e) and (f) $N = 4$ ZGNR.

Figure 2 shows the transmission coefficient and band structure of three ZGNRs. As for the wide ZGNR with $N = 10$, the transmission coefficient is almost two except in some small energy range. In [−0.22 eV, −0.16 eV] and [0.16 eV, 0.22 eV], the transmission coefficient increases to four. The enhancement in transmission is mainly attributed to the edge state. As $\theta = 0°$, the two-probe device is actually a periodic structure with ferromagnetic order. So, the transmission is determined by the number of electronic states. In Fig. 2(b), one can find two electronic states in the range other than [−0.22 eV, −0.16 eV] and [0.16 eV, 0.22 eV] but four states in the ranges of [−0.22 eV, −0.16 eV] and [0.16 eV, 0.22 eV]. Similar behavior can be found in Figs. 2(c) and 2(d) for $N = 8$ ZGNR. As the width of ZGNR becomes small, i.e., $N = 4$ shown in Figs. 2(e) and 2(f), one can obviously see that the transmission curve shows many spikes in the ranges of [−0.22 eV, −0.16 eV] and [0.16 eV, 0.22 eV]. These spikes can be understood based on the band structure of $N = 4$ where the edge state is split. The splitting of the edge state is attributed to the coupling between the top and bottom edges. The wider the ZGNR is, the weaker the coupling between the two edges is and the smaller the splitting is.

Figure 3 shows the magnetization distribution of $N = 10$, $N = 8$, and $N = 4$ ZGNRs with different magnetic profiles on the two edges at $\theta = 180°$. For clarity, we use the symbol A/B to denote the magnetization distribution with the first symbol A and the second symbol B for the top and bottom edges. Here, the A and B could be either C (collinear) or X (helical). So, the C/C and X/X are for the common magnetization on the two edges as shown in Fig. 3. For the C/C, an abrupt domain wall, where magnetic moments change the direction in the center of the edge, can be seen clearly. As seen from the polar plot in Fig. 4, the sizes of most magnetic moments remain unchanged except in the central region. For the X/X, the magnetic moment changes its direction gradually. Compared to the C/C, the angle between two neighboring magnetic moments is small in the X/X, which results in a small Heisenberg exchange energy. This has been validated by previous calculations based on the periodic unit cell of the ZGNR.[32]

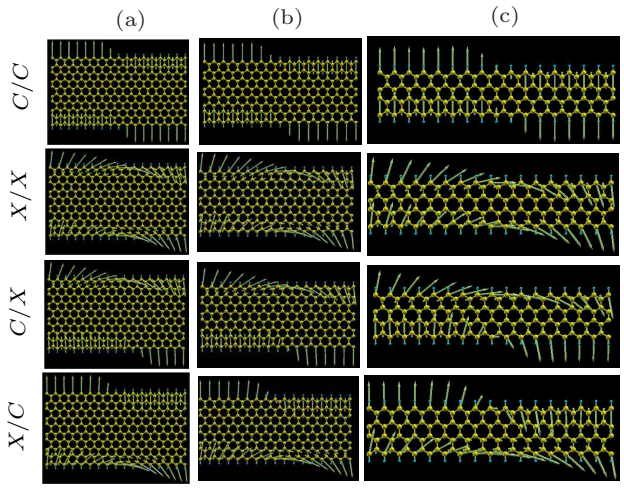


Fig. 3. Magnetization distributions of (a) $N = 10$, (b) $N = 8$, and (c) $N = 4$ ZGNRs at $\theta = 180°$. The symbol A/B denotes magnetization A on top edge and magnetization B on bottom edge. C and X denote collinear and helical magnetization distributions, respectively.

As for the X/C or C/X, the top and bottom edges are of different magnetization distributions. In self-consistent iteration, it can reach a converged configuration, indicating that such magnetization distribution represents a local minimum in energy landscape. This is the main result in this paper. Compared to the C/C and X/X, the X/C or C/X ZGNR has almost the same helical magnetization which can be appreciated in Fig. 4. The size and orientation of magnetic moments in helical magnetization are the same as the C/C and X/X. However, the abrupt domain wall changes a lot. Especially, the orientation of magnetic moments of the abrupt domain wall in the X/C or C/X ZGNR is no longer collinear, but tilted with respect to the z axis. This is mainly arisen from the coupling between the top and bottom edges, which is obvious for $N = 4$ ZGNR. In $N = 4$ and X/C ZGNR, the helical domain wall (top) presents the usual behavior but the abrupt domain wall (bottom) presents a small domain wall near the central region. This can be appreciated from its polar plot in Fig. 4 (X/C (bottom)) with magnetic moments gradually rotated. In such narrow ribbon, the coupling between the top and bottom edges

is strong. It reproduces a tendency that both top and bottom edges approach the helical magnetization distribution. Here, it should be understood that the symbol C may be inappropriate since it is not strictly collinear.

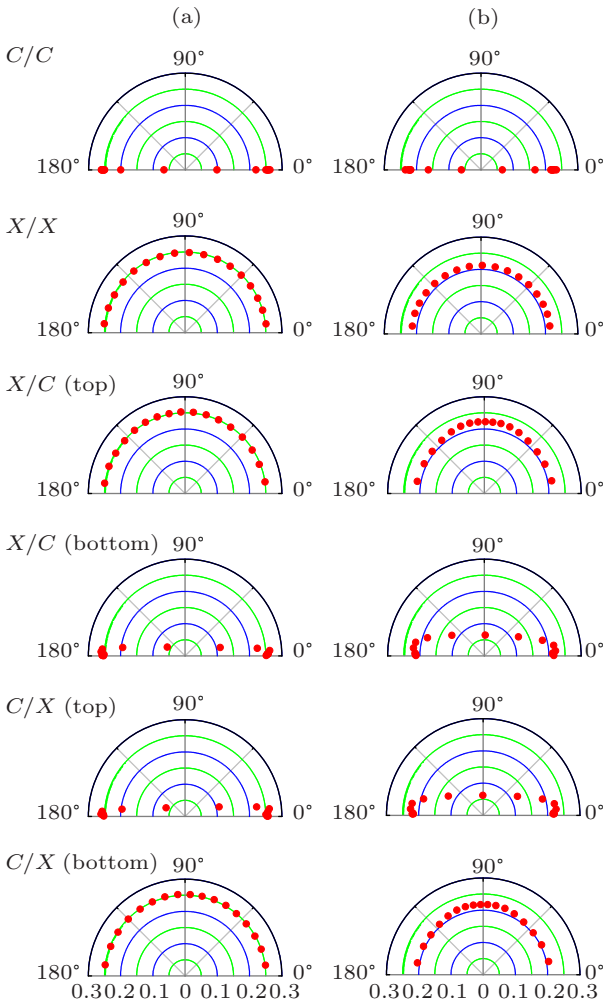


Fig. 4. Polar plot of the direction and size of local magnetic moments along the transport direction at $\theta = 180°$ for (a) $N = 8$ and (b) $N = 4$ ZGNRs. Only the magnetic moments of carbon atoms on the top and bottom edges are shown. Each point corresponds to an carbon atom on the edge. The size of magnetic moment is represented by the length from the sphere to the center of circle. The unit of magnetic moment is μ_B. The direction of magnetic moment is represented by the azimuth from the vertical line to the sphere in the polar plot.

We next discuss the transmission in the above-mentioned ZGNRs at $\theta = 180°$ shown in Fig. 5. As for the C/C and X/X, the X/X ZGNR shows similar behavior to $\theta = 0°$ shown in Fig. 2. Although the helical ($\theta = 180°$) and ferromagnetic ($\theta = 0°$) orders are quite different, the spin scattering mechanism is similar. In helical magnetism, the angle between neighboring magnetic moments is small. The spin scattering from one moment to its nearest neighboring moment is weak, i.e., the spin mixing effect. But for the C/C ZGNR, the abrupt reverse of magnetic moments near the center of the edges induces a strong spin-flip scattering and increases the resistance. As for the X/C or C/X ZGNR, the transmission near the Fermi level lies between those of C/C and X/X. This is because the spin transport is blocked in the abrupt domain wall while switched on in another helical domain wall. The relationship of transmission can be concluded with an approximate formula

$$T_{C/X} = T_{X/C} = (T_{C/C} + T_{X/X})/2. \quad (1)$$

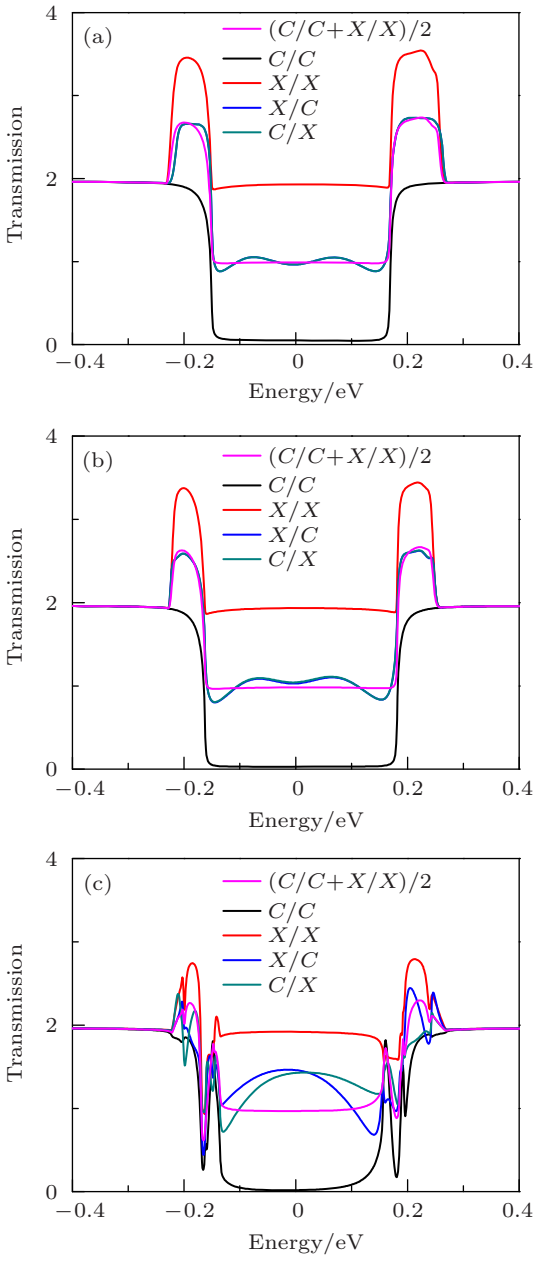


Fig. 5. Transmission versus energy for (a) $N = 10$, (b) $N = 8$, and (c) $N = 4$ ZGNRs at $\theta = 180°$.

When the ZGNR becomes narrow, the transmission develops many details, e.g., spikes shown in Fig. 5(c). The spikes are closely related to the coupling between the top and bottom edges. Moreover, equation (1), which holds for $N = 10$ and $N = 8$ ZGNR, is no longer suitable for $N = 4$ ZGNR. Especially near the Fermi level, the violation is remarkable. This implies that a wide ZGNR is better for the situation where the inter-edge coupling needs to be avoided. Since the transmission curves of $N = 10$ and $N = 8$ ZGNRs behave similarly,

we believe that above the width of $N = 10$ the effect of inter-edge coupling on transmission would be negligible. These results of spin transport would be of significance in the design of ZGNR-based spintronic devices. For instance, one can obtain the transmission coefficient of zero, one, and two with the C/C, C/X, and X/X ZGNRs, respectively.

Finally, we will discuss a potential route to realize distinct magnetizations on the two edges. First, one believes that a wide ZGNR is desired. In a wide ZGNR, the inter-edge coupling can be neglected and thus one can tune the magnetization of the edges independently. Second, as the helical domain wall is energetically lower than the abrupt one, it is possible to first obtain the helical domain wall on the two edges. Our previous calculations have demonstrated that the helical domain wall can collapse to an abrupt domain wall in the presence of adsorbates or atom substitution on the edge.[42,43] So, one can introduce impurities into one of the edges to destroy the helical domain wall on this edge.

Moreover, the fabrication of 180° domain wall under study can be made possible in a similar way to that used in Fe/MgO/Fe magnetic tunnel junction. First, a static magnetic field is applied to the ZGNR to induce uniform magnetization in the left and right leads. Then, we can attach an antiferromagnet to the right lead. Based on the well-known exchange bias effect,[44] such an antiferromagnet will pin the magnetization of the right lead to a direction antiparallel to the left lead, producing a 180° domain wall.

4. Conclusion

We calculated the magnetization distribution and transmission coefficient of the ZGNR with distinct magnetic profiles on two edges based on first-principles calculations. The systems under consideration are a wide $N = 10$, 8, and a narrow $N = 4$ ZGNRs. As for the wide ZGNR, the helical domain wall on the top (bottom) edge and the abrupt domain wall on the bottom (top) edge can survive. But for a narrow ZGNR, the coupling between the two edges results in the correlation between the two edge magnetizations. The abrupt domain wall on one edge is of helical characteristics near the center of the edge. This changes the band structure and spin transport greatly. The transmission curve of unequal magnetization distribution lies between those of equal C/C and X/X ZGNRs. The spin transport behavior of a wide ZGNR can be described by a formula. The formula indicates that, by tuning the edge magnetization, the transmission of zero, one, and two can be realized. Moreover, when the width is small, the coupling between the two edges induces many details, i.e., spikes in the transmission curve. The coupling makes the separation of the top and bottom edge states difficult and thereby invalidate the above-mentioned formula. The results reported here may find potential applications for ZGNR-based spintronic devices.

References

[1] Geim A K and Novoselov K S 2007 *Nat. Mat.* **6** 183
[2] Casto Neto A H, Guinea F and Peres N 2013 *Rev. Mod. Phys.* **81** 109
[3] Zhou J, Hu T, Dong J M and Kawazoe Y 2012 *Phys. Rev. B* **86** 035434
[4] Chen M X, Zhong Z and Weinert M 2016 *Phys. Rev. B* **94** 075409
[5] Chen M X and Weinert M 2016 *Phys. Rev. B* **94** 035433
[6] Ju W, Wang D, Li T, Wang H, Zhou Q, Xu Y, Li H and Gong S 2020 *J. Phys.: Condens. Mat.* **32** 175503
[7] Cui P, Zhang Q, Zhu H B, Li X X, Wang Y W, Li Q X, Zen C G and Zhang Z Y 2016 *Phys. Rev. Lett.* **116** 026802
[8] Pachoud A, Ferreira A, Ozyilmaz B and Castro Neto A H 2014 *Phys. Rev. B* **90** 035444
[9] Xiao D, Liu G, Feng W, Xu X and Yao W 2012 *Phys. Rev. Lett.* **108** 196802
[10] Feng W, Yao Y, Zhu W, Zhou J, Yao W and Xiao D 2012 *Phys. Rev. B* **86** 165108
[11] Huang B, Liu F, Wu J, Gu B L and Duan W 2008 *Phys. Rev. B* **77** 153411
[12] Gmitra M and Fabian J 2015 *Phys. Rev. B* **92** 155403
[13] Zhang W, Hajiheidari F and Mazzarello R 2017 *Phys. Rev. B* **96** 245413
[14] Fujita M, Wakabayashi K, Nakada K and Kusakabe K 1996 *J. Phys. Soc. Jpn.* **65** 1920
[15] Bai Z, Shen L, Cai Y, Wu Q, Zeng M, Han G and Feng Y P 2014 *New J. Phys.* **16** 103033
[16] Lee J and Fabian J 2016 *Phys. Rev. B* **94** 195401
[17] Okada s and Oshiyama A 2001 *Phys. Rev. Lett.* **87** 146803
[18] Sawada K, Ishi F, Saito M, Okada S and Kawai T 2009 *Nano Lett.* **9** 269
[19] Jung J, Pereg-Barnea T and MacDonald A H 2009 *Phys. Rev. Lett.* **102** 227205
[20] Padilha J E, Pontes R B and da Silva A J R 2013 *Solid State Commun.* **173** 24
[21] Meunier V, Souza Filho A G and Barros E B 2016 *Rev. Mod. Phys.* **88** 025005
[22] Yazyev O and Katsnelson M I 2008 *Phys. Rev. Lett.* **100** 047209
[23] Biel B, Blase X, Triozon F and Roche S 2009 *Phys. Rev. Lett.* **102** 096803
[24] Tombros N, Jozsa C, Popinciuc M, Jonkman H T and van Wees B J 2007 *Nature* **448** 571
[25] Li Z, Qian H, Wu J and Duan W H 2008 *Phys. Rev. Lett.* **100** 206802
[26] Ozaki T, Nishio K, Weng H and Kino H 2010 *Phys. Rev. B* **81** 075422
[27] Oda T, Pasquarello A and Car R 1998 *Phys. Rev. Lett.* **80** 3622
[28] Wiesendanger R 2009 *Rev. Mod. Phys.* **81** 1495
[29] Bode M, Heide M, von Bergmann K, Ferriani P, Heinze S, Blugel S and Wiesendanger R 2007 *Nature* **447** 190
[30] Yao Y, Ye F, Qi X L, Zhang S C and Fang Z 2007 *Phys. Rev. B* **75** 041401
[31] Czerner M, Yavorsky B Y and Mertig I 2008 *J. Appl. Phys.* **103** 07F304
[32] Zhang Y, Yan X H, Guo Y D and Xiao Y 2017 *J. Appl. Phys.* **121** 174303
[33] http://www.openmx-square.org/ for the details of DFT/NEGF method as implemented in OpenMX
[34] Ozaki T and Kino H 2005 *Phys. Rev. B* **72** 045121
[35] Soler J M, Artacho E, Gale J D, Garcia A, Junquera J, Ordejon P and Sanchez-Portal D 2002 *J. Phys.: Condens. Matter* **14** 2745
[36] Taylor J, Guo H and Wang J 2001 *Phys. Rev. B* **63** 121104
[37] Rungger I and Sanvito S 2000 *Phys. Rev. B* **78** 035407
[38] Brandbyge M, Mozos J, Ordejón P, Taylor J and Stokbro K 2002 *Phys. Rev. B* **65** 165401
[39] Zutic I, Fabian J and Das Sarma S 2004 *Rev. Mod. Phys.* **76** 323
[40] Kubler J, Hock K H and Sticht J 1988 *J. Phys. F* **18** 469
[41] Burton J D, Sabirianov R F, Jaswal S S and Tsymbal E Y 2006 *Phys. Rev. Lett.* **97** 077204
[42] Liang J T, Yan X H, Zhang Y, Guo Y D and Xiao Y 2019 *J. Mag. Mag. Mat.* **480** 101
[43] Press M R, Liu F, Khanna S N and Jena P 1989 *Phys. Rev. B* **40** 399
[44] Nogues J and Schuller I K 1999 *J. Mag. Mag. Mat.* **192** 203